



Heterogeneous phototransformation of halogenated polycyclic aromatic hydrocarbons: influencing factors, mechanisms and products

Yueyao Yang^{1,2,3}, Yahui Liu^{1,2,3}, Guohua Zhu², Bingcheng Lin², Shanshan Zhang^{1,2,3}, Xin Li^{1,2,3}, Fangxi Xu⁴, He Niu⁴, Rong Jin², and Minghui Zheng^{1,2,3}

¹State Key Laboratory of Environmental Chemistry and Ecotoxicology, Research Center for Eco-Environmental Sciences, Chinese Academy of Sciences, Beijing, 100085, China

²School of Environment, Hangzhou Institute for Advanced Study, University of Chinese Academy of Sciences, Hangzhou, 310024, China

³College of Resource and Environment, University of Chinese Academy of Sciences, Beijing, 100049, China

⁴Zhejiang Taizhou Ecological and Environmental Monitoring Center, Taizhou, 318000, China

Correspondence: Rong Jin (jinrong@ucas.ac.cn)

Received: 8 September 2024 – Discussion started: 22 October 2024

Revised: 12 February 2025 – Accepted: 14 February 2025 – Published: 9 April 2025

Abstract. Chlorinated and brominated polycyclic aromatic hydrocarbons (XPAHs) are emerging pollutants widely found in atmospheric particulate matter (PM). However, their environmental transformation mechanisms remain poorly understood. In this study, we collected PM samples of varying sizes over a year for XPAH analysis and found that the average concentrations of XPAHs peaked in winter and were dominated by the contribution of PM₁ (particulate matter $\leq 1 \mu\text{m}$ in aerodynamic diameter) (47.0 %). Correlation analysis with relevant meteorological parameters showed strong associations between XPAH fluctuations and PM, temperature and humidity. Hence, controlled laboratory experiments were conducted to explore the influence of particle size, sunlight duration, temperature, humidity and oxidant concentrations on XPAHs. Our results indicated that the transformation rates of XPAHs were influenced by the parent polycyclic aromatic hydrocarbon structures (with phenanthrene < fluoranthene < pyrene < benz[a]anthracene \approx anthracene < benzo[a]pyrene) as well as the substitution of halogens (chlorinated < brominated). Furthermore, the photoirradiation promoted the heterogeneous transformation of XPAHs; this process was accelerated by the increased concentrations of reactive oxygen species and elevated temperature, peaking at a humidity level of 45 %. The transformation products were identified by non-target analysis. According to that, we then proposed phototransformation pathways for XPAHs, suggesting a mechanism involving dehalogenation followed by oxidation. Predictions were made regarding the persistence, bioaccumulation, long-range transportation, and toxicities of XPAHs and their transformation products, showing a decrement in environmental risk as the transformation progressed. This study provides novel insights into the primary influencing factors for particulate XPAH variations and the mechanisms of heterogeneous phototransformation.

1 Introduction

Chlorinated and brominated polycyclic aromatic hydrocarbons (hereafter CIPAHs and BrPAHs, respectively), cumulatively referred to as XPAHs, are halogenated derivatives of polycyclic aromatic hydrocarbons (PAHs) that have gained considerable attention in recent years due to their heightened persistence, toxicity and bioaccumulation relative to their parent PAHs (Jin et al., 2017b; Ma et al., 2013; Ohura et al., 2013; Nishimura et al., 2017). At present, research on XPAHs primarily encompasses the following aspects: (1) the establishment of pretreatment and instrumental methods (Takikawa et al., 2023; Sei et al., 2021; Noro et al., 2023; Jin et al., 2023; Liu et al., 2019b), (2) environmental detection across various environmental media (Jin et al., 2020; Xie et al., 2021), and (3) the identification of anthropogenic sources. XPAHs have been reported to exist in the air (Nilsson and Ostman, 1993; Kakimoto et al., 2014; Jin et al., 2017a), soil (Sun et al., 2013; Zhang et al., 2006), water (Shiraishi et al., 1985), sediment (Ohura et al., 2015) and organisms (Jin et al., 2017c; Nishimura et al., 2017; Liu et al., 2019b; Xia et al., 2019; Ohura et al., 2015). Their sources, such as industrial thermal processes (Yang et al., 2022b), electronic waste decomposition (Wang et al., 2022) and vehicular emissions (Deng et al., 2023), have been identified, by means of the detection of XPAHs in the stack gas and fly ash emitted from these sources (Jin et al., 2017b; Nishimura et al., 2017; Yang et al., 2022a). However, a significant aspect of research appears to have been overlooked, i.e., their environmental transformation. Variations in the transformation mechanisms of XPAH congeners in environmental matrices can result in differences in their environmental fate and associated risks.

Photochemical processes have been verified to represent a marked elimination pathway for organic substances affecting the atmosphere (Hu et al., 2021; Malecha and Nizkorodov, 2016; Laskin et al., 2015). For example, PAHs have been confirmed to undergo oxidation (Zhu et al., 2022) or become subject to fragmentation (Zhang et al., 2024; Hu et al., 2021) via atmospheric photochemical reactions. Therefore, despite the absence of direct study, given their structural similarities to PAHs, XPAHs also possess the potential to undergo similar processes. Studies by Ohura et al. (2008) have also confirmed the photochemical transformation of CIPAHs when they are exposed to light in cyclohexane solvent. Field observations provided additional evidence, suggesting that photochemistry plays a crucial role in atmospheric XPAH transformation. For instance, certain studies have shown that concentrations of CIPAHs in particulate matter (PM) were slightly higher at nighttime than during daytime (Ma et al., 2013; Ohura et al., 2013), indicating that daytime photochemistry contributed to the transformation of XPAHs. For BrPAHs, although no direct nighttime versus daytime concentration comparison has been conducted, prior research has indicated

that BrPAHs might exhibit greater instability under photoirradiation than CIPAHs (Ohura et al., 2009).

Heterogeneous reactions were identified to be the key mechanisms driving the transformation of atmospheric organic compounds, e.g., PAHs (Jia et al., 2019), during these photochemistry processes (Zhang et al., 2023). Atmospheric PM acts as a significant carrier for both environmental pollutants and catalysts, serving as a medium for heterogeneous reactions. These reactions could be influenced by various environmental factors. For instance, reactive oxygen species (ROSS) have been identified to accelerate the phototransformation of polychlorinated naphthalene (PCN) species, which are two-ring CIPAHs, on the surface of silica gel (Kang et al., 2021). In addition, the temperature and humidity have been noted to influence the lifetime of atmospheric organics (Shiraiwa et al., 2011). For example, the heterogeneous oxidation mechanisms of organophosphate flame retardants were found to be significantly affected by humidity (Liu et al., 2019a). In the case of particulate XPAHs, heterogeneous reactions may also play a crucial role in their transformation. However, the influencing factors, specific mechanisms, pathways and products remain unclear, necessitating further exploration.

This study aims to unravel the mechanisms, influencing factors, pathways and products of XPAH heterogeneous transformation on PM. To achieve this, we conducted field studies that were complemented by meticulously designed laboratory experiments and nontarget organic compound analysis. Initially, we collected annual-range particle samples of various sizes along with relevant meteorological data. These samples were subsequently analyzed for XPAHs. Through multivariate parameter analysis, we explored XPAH fluctuations correlated with meteorological data to pinpoint key influencing factors. Subsequently, controlled laboratory experiments were designed and conducted to unveil the heterogeneous transformation of XPAHs under the influence of particle size, humidity, temperature and atmospheric oxidant content. The persistence, bioaccumulation, long-range transportation and toxicities of the transformation products were then assessed to determine the environmental risks associated with XPAH transformation. Therefore, the findings of this study contribute comprehensive insights into the mechanisms and environmental risk involved in the fate of XPAHs in the environment.

2 Materials and methods

2.1 Experimental materials

In this study, a comprehensive investigation was conducted on 41 XPAHs with two to five benzene rings, along with an analysis of the corresponding parent PAHs. The parent PAHs are abbreviated as follows: Nap (naphthalene), Phe (phenanthrene), Ant (anthracene), Triph (triphenylene), Fluor (fluoranthene), Pyr (pyrene), BaA (benz[a]anthracene) and BaP (benzo[a]pyrene). The congeners in the CIPAH and

BrPAH groups are described as Cl-, Cl₂-, Cl₃-, Cl₄-, Br- and Br₂-, indicating the presence of monochlorinated, dichlorinated, trichlorinated, tetrachlorinated, monobrominated and dibrominated PAH derivatives, respectively, with the numbers denoting the substituting positions. Specific names, abbreviations, and molecular structures of 20 CIPAHs and 21 BrPAHs are listed in Table S1 in the Supplement. As reported in our previous study (Jin et al., 2017a), standards, isotopically labeled internal standards, and recovery standards for XPAHs and PAHs were commercially obtained.

2.2 Sample collection and extraction

Atmospheric particles of three sizes (PM₁, PM_{2.5}, and PM₁₀, defined as particulate matter with aerodynamic diameters ≤ 1 , ≤ 2.5 , and ≤ 10 μm , respectively) were collected in Hangzhou from March 2023 to February 2024 using medium-flow samplers (Wuhan Tianhong Instruments Co., Ltd., China). These samplers were positioned atop a school building at a height of approximately 15 m above ground level. The sampling site (30°8'15" N, 120°4'17" E) was situated in the Xihu District of Hangzhou, with no industrial area within a 5 km radius. Samples were collected in monthly cycles, at a flow rate of 0.1 m³ min⁻¹. Quartz-fiber filters were employed to capture particles. Subsequently, samples were collected, dried, weighed and stored at -18 °C.

Samples were extracted with a mixture of dichloromethane and hexane (1 : 4, *v* : *v*) by an automatic Soxhlet extractor (UniversalExtractor E-800, Buchi, Germany). The extracted samples were then purified using an active-silica column and concentrated to 50 μL using a rotary evaporator and nitrogen blower. Specific processes for the extraction and cleanup processes can be found in our previous study (Jin et al., 2017a).

2.3 Experimental design for the heterogeneous transformation of particulate XPAHs

In this study, we designed a phototransformation device that provided complete confinement and precise control over the experimental conditions. The reaction unit employed a xenon lamp (light intensity: 100 mW cm⁻²; luminous efficacy: 100 lm W⁻¹) as the primary light source with an AM1.5 filter, which can achieve a good fit with the sunlight spectrum, effectively simulating outdoor solar radiation (the average luminous efficacy ranged from 100 to 120 lm W⁻¹ at noon at the sampling sites) (Cao et al., 2020; Wang et al., 2020). The entire photolysis reaction unit comprises a gas supply, mass flowmeters, a dryer (with molecular sieve and colored silica gel), a bubbler containing Milli-Q water, a xenon lamp, an optical reactor, a quartz reaction vessel, a temperature control system, gas absorption bottles and a relative humidity monitoring component (Fig. 1a). To accurately emulate atmospheric conditions, model particles and a composite mixture comprising 41 XPAHs were meticulously pre-

pared. Sequentially, 20 μL of the XPAH mixture (1 mg L⁻¹) or individual congener solution was deposited onto the surface of the prepared layer of silica particles ($M_{\text{XPAHs}}: M_{\text{PM}} = 2 \mu\text{g g}^{-1}$) (Fig. 1b and Fig. S1 in the Supplement). The settings of the concentrations were based on previous studies on the XPAH concentration per particle mass (Jin et al., 2018, 2017c). Specific information on the devices and experiments are described in Sect. S1 in the Supplement.

To comprehensively explore the impact of various factors, including particle sizes (100 nm, 2 μm and 10 μm), temperatures (10, 20 and 30 °C), humidity (RH = 30 %, 45 % and 60 %), oxidant concentrations (H₂O₂ was selected for its representativeness among reactive oxygen species and ease of control, 0 % (no H₂O₂ was added to the system, while tert-butyl alcohol (TBA) was introduced), 0 %, 1 %, 3 %, 5 % and 10 %) and irradiation duration (0, 10, 30, 60 and 180 min) on the phototransformation mechanism of XPAHs, a series of experiments were conducted (Sect. S1). The reacted gas was directed into a toluene solution for the analysis of XPAHs in the tail gas, with less than 1 % of the XPAHs escaping through volatilization during the reaction time. Dark control groups were conducted in each experiment to ensure that the difference between the two sets of experiments was due to the transformation effect caused by photoirradiation. Upon completion of the reactions, the particle layer within the reaction vessel was sonicated with 200 μL of toluene, followed by centrifugation of the supernatant. The resulting solution was then transferred into a centrifuge tube for subsequent product analysis.

2.4 Instrumental analysis

Analysis of the XPAHs and PAHs was conducted using gas chromatography coupled with magnetic sector high-resolution mass spectrometry (HRGC-HRMS; DFS, Thermo Fisher Scientific, USA) equipped with an electron ionization source. Specific information on the parameters for the oven and mass spectrometer (MS) can be found in our previous study (Jin et al., 2017c). The analytical program and instrumental parameters for the analysis of PAHs were set according to "CalEPA Method 429".

Nontarget analysis of the transformation products of XPAHs was performed using a TRACE 1310 GC coupled to a quadrupole-Orbitrap MS (Thermo Fisher Scientific, USA). Data were collected and processed using Thermo Scientific TraceFinder 5.1 software. High-resolution mass spectra of unknown compounds were deconvoluted into pure spectra using the Deconvolution plugin of TraceFinder software and then verified against the standard mass spectra from the commercial library NIST 2014. Specific information on the nontarget analysis is shown in Sect. S2.

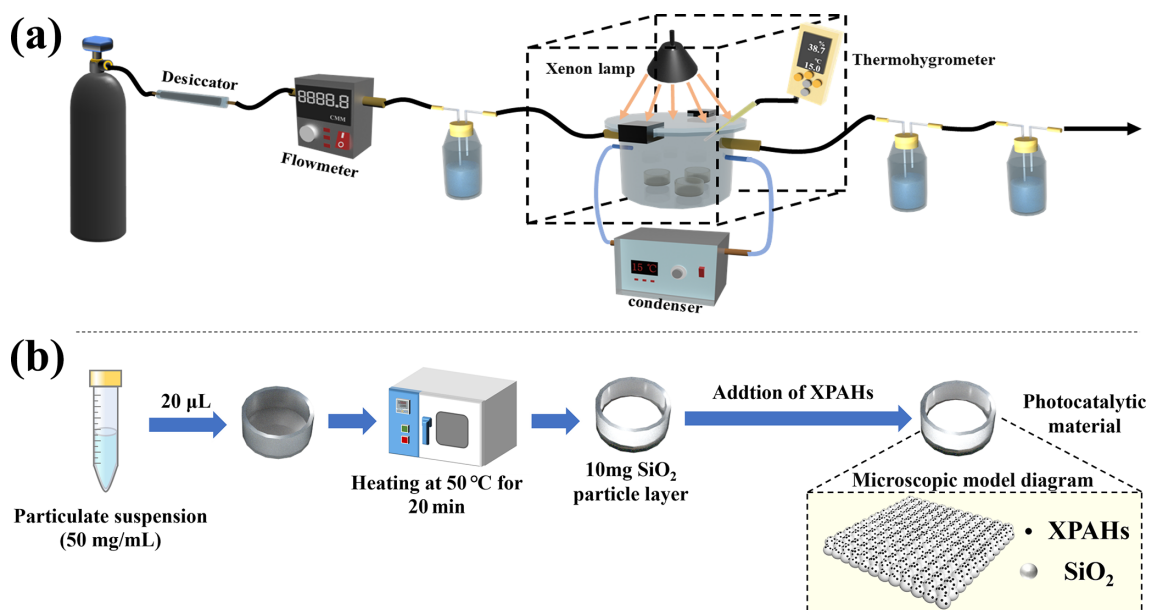


Figure 1. The (a) laboratory photochemical transformation setup and (b) particulate matter preparation process.

2.5 Environmental behavior and toxicity assessment of XPAHs and their transformation products

To assess the ecological risk and environmental characteristics – specifically, persistence, long-range transport potential and bioaccumulation – of transformation products of XPAHs, this study employed the KOWWIN, KOAWIN, BCFBAF and Level III fugacity models within EPI Suite 4.1 to compute the various physicochemical properties of compounds. Essential environmental parameters including the molecular weight; the octanol–water partitioning coefficient (K_{ow}); the air–water partitioning coefficient (K_{aw}); and the half-lives in air, water and soil were subsequently introduced into the Pov-LRTP tool, which was used to estimate overall persistence and long-range transport potential in the environment (Concha and Manzano, 2023). Subsequently, the P-B-LRTP score was developed based on persistence (Pov), characteristic travel distance (CTD) and transfer efficiency (TE) values to prioritize the screened compounds. The respiratory toxicity model in ProTox 3.0 (Banerjee et al., 2024) was used to predict the toxicity of the products, assessing their median lethal dose (LD50) and toxicity class.

$$\text{P-B-LRTP Score}_i = \text{LogPov} + \text{LogBAF} + \text{LogTE}$$

2.6 Quality assurance and quality control

For the analysis of actual atmospheric PM samples, the recovery rates of internal standards ranged from 52 % to 105 %. In laboratory simulation experiments, the recovery rates of XPAHs ranged from 78 % to 115 %, while those of PAHs ranged from 53 % to 120 %. These recovery rates met the requirements for the detection and analysis of persis-

tent organic pollutants. The limit of detection (LOD) values ranged from 0.17 to 1.9 fg m^{-3} for CIPAHs and from 0.23 to 1.6 fg m^{-3} for BrPAHs. The LODs for CIPAH or BrPAH monomers vary due to differences in chemical structures, properties and substituents, which influence their stability, response and signal intensity during analysis, ultimately affecting detection limits. A blank sample was analyzed together with each batch of samples, and the relative concentrations of all XPAH congeners were below the detection limits.

3 Results and discussion

3.1 Occurrence levels and congener profiles of particulate XPAHs

During the sampling period, PM concentrations ranged from 41.5 to 653 $\mu\text{g m}^{-3}$, with an average concentration of 130 $\mu\text{g m}^{-3}$ (Fig. S2a). PM₁ had the highest proportion, with an average of 47.0 %, while the proportions of PM_{1–2.5} and PM_{2.5–10} were comparable. Notably, the peak concentration was recorded in April 2023. This surge coincided with a dust storm originating from the north, leading to heightened levels of suspended dust in the atmosphere and a significant spike in PM levels. Barring exceptional weather conditions, PM concentrations in other seasons were approximately twice as high as those observed in the summer and autumn.

The concentrations of $\sum_{21}\text{CIPAHs}$ in the particles ranged from 0.60 to 61.5 pg m^{-3} (mean: 12.1 pg m^{-3}), while those of $\sum_{18}\text{BrPAHs}$ ranged from ND (not detected) to 5.40 pg m^{-3} (mean: 0.6 pg m^{-3}) during the sampling period (Fig. 2a). These values are lower than those reported in previous studies, such as Beijing, China

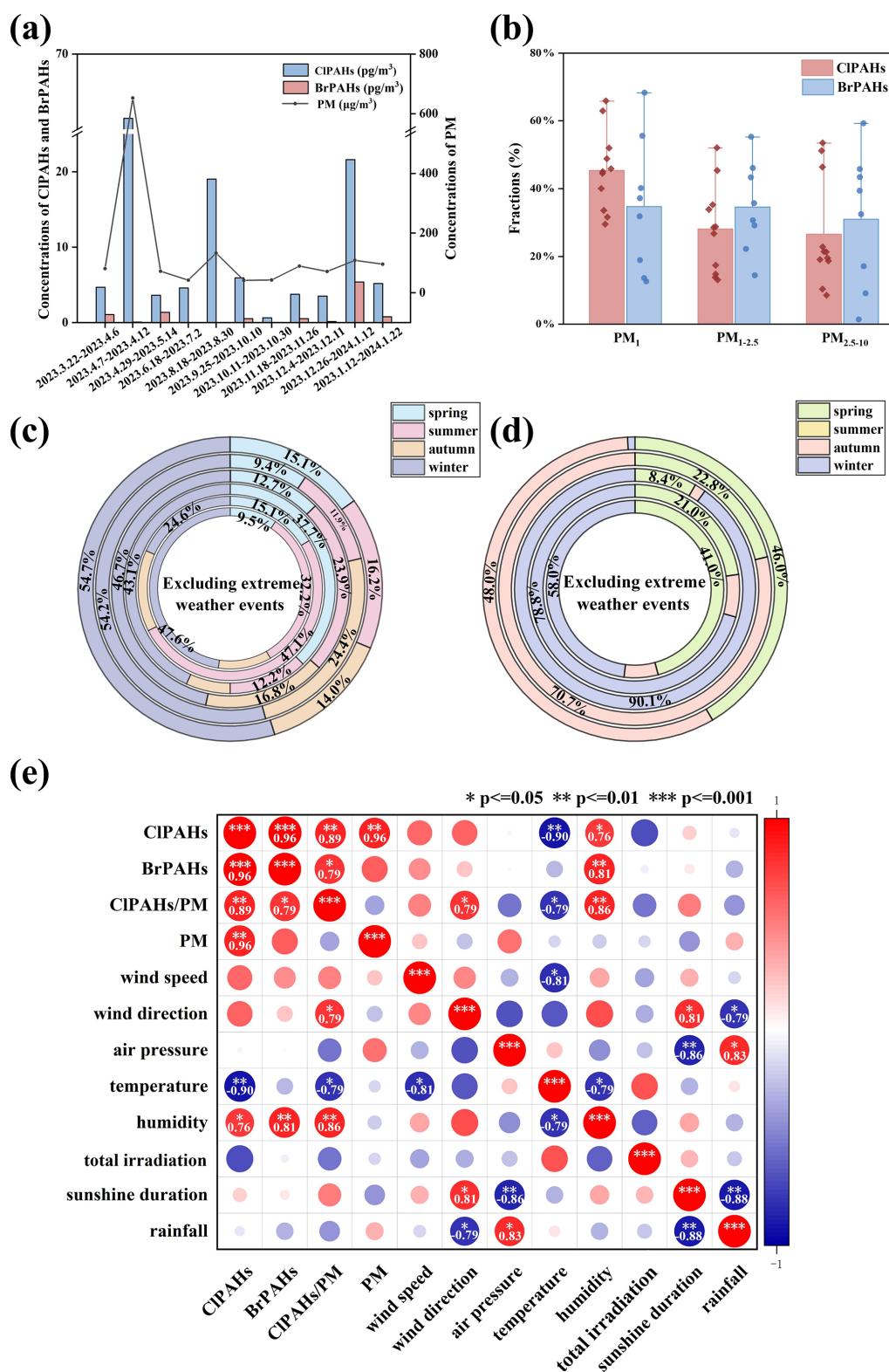


Figure 2. (a) The fluctuations in the concentrations of PM, \sum_{21} CIPAHs and \sum_{19} BrPAHs in the atmosphere. (b) The proportions of CIPAHs and BrPAHs across different PM diameters. (c, d) Seasonal distributions of CIPAH (c) and BrPAH (d) congeners, excluding events with extreme conditions, arranged from the outermost to innermost layers as follows: CIPhe, ClAnt, CIPyr, ClFluor, ClBaA and ClBaP; BrPhe, BrAnt, BrPyr, BrTriph and BrBaA. (e) A Pearson correlation analysis between CIPAHs, BrPAHs and CIPAHs/PM with meteorological parameters (wind speed, wind direction, air pressure, temperature, humidity, total radiation, sunshine duration and rainfall) under non-extreme weather conditions.

(\sum_{19} CIPAHs: 129 pg m^{-3} ; \sum_{19} BrPAHs: 9.50 pg m^{-3}) (Jin et al., 2017c); Ulsan, South Korea (\sum_{11} BrPAHs: 1.62 pg m^{-3}) (Vuong et al., 2020); and Shizuoka, Japan (\sum_{20} CIPAHs: 133 pg m^{-3}) (Ohura et al., 2013). With respect to their distribution in particles of different sizes, CIPAHs had the highest fraction in PM_{10} (mean: 45.4%; range: 29.4%–65.9%) and comparable proportions in $\text{PM}_{1-2.5}$ (mean: 28.1%; range: 13.0%–52.0%) and $\text{PM}_{2.5-10}$ (mean: 26.5%; range: 8.46%–53.5%). Conversely, BrPAHs showed no significant variance across the three particle size ranges, with concentrations of PM_{10} (mean: 35.9%; range: 12.5%–68.2%), $\text{PM}_{1-2.5}$ (mean: 35.7%; range: 14.3%–55.2%) and $\text{PM}_{2.5-10}$ (mean: 28.4%; range: 1.25%–59.2%) (Fig. 2b). In total, over 70% of XPAHs were bound to particles with diameters smaller than $2.5 \mu\text{m}$.

Concentration trends in XPAH homologue groups were as follows: ClFluor > ClBaP > ClAnt > ClPyr > ClPhe > ClBaA (Table S2); BrPyr > BrPhe > BrAnt > BrTriph > BrBaA > BrFluor (ND) (Table S3). The distribution profiles of XPAH congeners in PM_{10} in Hangzhou are shown in Fig. S2b and c and in Table S4. Among CIPAHs, 2-ClPhe/9-ClPhe, 1,5-Cl₂Ant/9,10-Cl₂Ant, 1-ClPyr, 3-ClFluor, 3,8-Cl₂Fluor and 6-ClBaP were found to be predominant throughout the year. These distributions aligned with findings of prior studies (Jin et al., 2017c; Kitazawa et al., 2006; Ma et al., 2013). It is worth noting that 6-ClBaP, characterized by the highest molar mass and highest toxic equivalent factor within the CIPAHs investigated in our study, demonstrated the highest concentration proportion. BrPAHs are predominantly constituted by 2-BrPhe, 9-BrPhe, 7-BrBaA and 1,6-Br₂Pyr. This represented a notable difference from previous literature, which predominantly identified 3-BrFluor, 1,8-Br₂Ant and 1-BrPyr as the primary congeners of BrPAHs in atmospheric PM in Beijing (Jin et al., 2017c). This disparity underscores variances in their respective sources or transformations.

3.2 Key environmental factors influencing temporal variations in particulate XPAHs

Extreme weather events such as sandstorms and prolonged light rainfall have been excluded in the following discussion. The average concentrations of PM and BrPAHs reached their nadirs during summer and autumn, while showing higher levels in the spring and the winter (Fig. S2d). Conversely, CIPAH concentrations remained relatively stable during the spring and the summer, decreased in the autumn, and peaked in the winter. The seasonal characteristics of CIPAHs with different parent PAH structures also varied (Fig. 2c). Except for ClBaA, the remaining CIPAHs reached their highest concentrations during the winter. ClFluor showed elevated concentrations in both the spring and the winter, whereas ClAnt demonstrated higher concentrations in the autumn and the winter. ClPhe maintained relatively consistent concentrations across the remaining three seasons. The seasonal characteris-

tics of CIPAHs and BrPAHs (Fig. 2d) also differed. Concentrations of BrPAHs varied significantly with season, with no congener detected in the summer and high concentrations of BrPhe, BrAnt and BrPyr in the spring and the winter, likely influenced by climatic conditions such as temperature and sunshine. This disparity can be attributed to the ease of generation from sources and the greater atmospheric stability of CIPAHs, while BrPAHs may be subjected to influences from atmospheric processes (Ohura et al., 2009).

Eight meteorological parameters were collected throughout the sampling period: wind speed, wind direction, air pressure, temperature, humidity, total irradiation, sunshine duration and rainfall. Details are listed in Table S5, and the results of multifactor correlation analysis are shown in Fig. 2e. A Pearson correlation analysis revealed significant positive correlations between CIPAHs and BrPAHs ($P < 0.001$, $R = 0.96$), PM ($P < 0.01$, $R = 0.96$), and humidity ($P < 0.05$, $R = 0.76$). BrPAHs exhibited a significant positive correlation with humidity ($P < 0.01$, $R = 0.81$). The impact of humidity was notably significant, as an increase in humidity tended to facilitate the upward adsorption of XPAHs onto PM. However, a previous study (Vuong et al., 2020) from Ulsan (South Korea) reported a negative correlation between humidity and XPAHs. This observation suggested that the relationship between XPAHs and humidity varied across different regions. Additionally, CIPAHs show a significant negative correlation with temperature ($P < 0.01$, $R = -0.90$), suggesting that higher temperatures corresponded to lower CIPAH concentrations. This further elucidated the phenomenon of lower CIPAH levels observed during the summer and autumn seasons. Other meteorological factors did not show significant correlations with CIPAHs or BrPAHs ($P > 0.05$), possibly due to the intricate interplay of multiple factors under natural conditions. Hence, the specific roles of meteorological conditions, such as sunlight intensity, duration of sunshine, temperature and humidity, warranted further investigation.

3.3 General transformation mechanisms of particulate XPAHs under photoirradiation

According to both preliminary research (Li et al., 2023) and the experimental results mentioned above, it is evident that meteorological conditions can significantly impact the concentrations and distributions of XPAHs on PM. Controlled laboratory experiments were conducted in this study to unveil the heterogeneous transformation mechanisms of XPAHs.

The transformation ratios of XPAHs were calculated based on the ratios of transformed XPAHs to the initial concentration ($(C_0 - C_t)/C_0$). With the increase in the irradiation time, a general trend in transformation was observed across XPAH congeners (Fig. 3). Overall, the transformation rates of CIPAHs appeared to adhere to the following sequence: ClPhe < ClFluor < ClPyr < ClBaA \approx ClAnt < ClBaP (Fig. S3). This pattern aligned with the previously re-

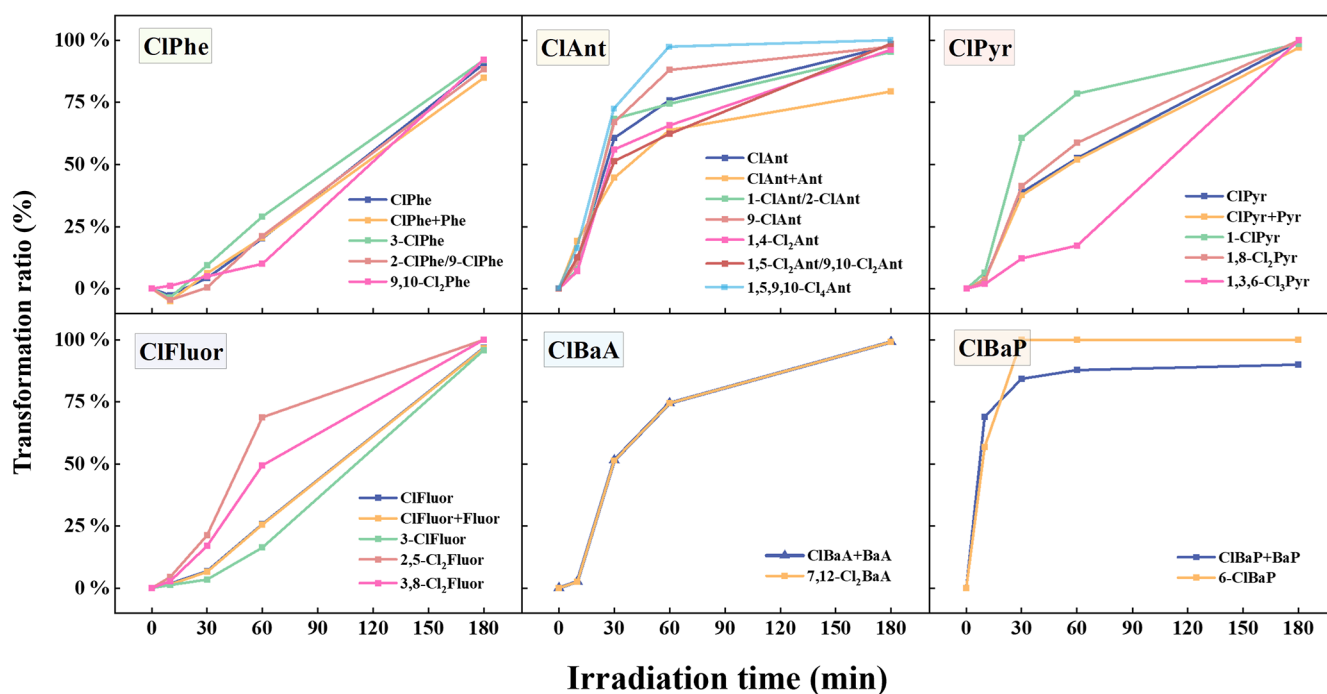


Figure 3. Relationships between the transformation ratios of CIPAHs and photoirradiation time.

ported trends in PAH photolysis rates (Phe < BaA < Ant \approx BaP) (Zhao et al., 2017), indicating a strong influence from the parent PAH structures. In a combined consideration of CIPAHs and their parent PAHs, shown as “CIPAHs + PAHs” in Fig. S3, we also observed the formation of PAHs and decreases in the total concentrations of CIPAHs and PAHs. This indicated that there was the dechlorination of CIPAHs and the simultaneous fragmentation of parent PAH structures during the transformation of CIPAHs.

In addition, the substitution numbers of the structures had a strong influence on the transformation of CIPAHs: with increment of the substitution numbers, the transformation ratios progressively decreased (Fig. 3). For example, after 1 h of irradiation, transformation ratios were approximately 20 % for 3-CIPhe and 2-CIPhe/9-CIPhe, while they were 10 % for 9,10-Cl₂Phe. An exception was observed for ClAnt congeners (1,4-Cl₂Ant or 1,5-Cl₂Ant/9,10-Cl₂Ant < 1-ClAnt/2-ClAnt or 9-ClAnt < 1,5,9,10-Cl₄Ant). This difference could be attributed to the fact that the investigated low-chlorine-number ClAnts are dechlorination products of high-chlorine-number ClAnts. While the substitution position had some impact, it was not as significant as the number of chlorines. For instance, both 2,5-Cl₂Fluor and 3,8-Cl₂Fluor demonstrate comparable photolysis extents, with approximately 20 % transformation after 30 min of irradiation, and transformation ratios of 68.8 % and 49.4 % after 3 h of irradiation, respectively.

For BrPAHs (Fig. S4), the overall transformation ratio ranked as follows: BrPhe < BrAnt < BrPyr \approx BrFluor <

BrBaA < BrBaP. The transformation ratio ranking between BrPAHs and CIPAHs exhibited disparities, implying that distinct halogen substitutions might yield diverse transformation effects. BrPAHs degraded more rapidly than CIPAHs. For example, BrPyr degraded by 60 % after 30 min of irradiation, while ClPyr only degraded by less than 40 %. Additionally, the increase in the bromination degree did not appear to have a notable effect on the transformation rate of BrPAHs, which differed from CIPAHs.

3.4 Influencing factors for heterogeneous transformation of particulate XPAHs

The influencing factors, i.e., particle size, relative humidity, reactive oxygen species content and temperature, on XPAH transformation have been investigated (Sect. S1). Although previous studies have revealed variations in XPAH concentrations on particles of different sizes (Jin et al., 2017c; Lara et al., 2022; Ma et al., 2013), the influence of particle size (100 nm, 2 μ m and 10 μ m) on transformation efficiency was found to be not notably significant in simulated experiments (Fig. S5 and Sect. S3).

The influence of humidity varied among CIPAHs with different parent structures (Fig. 4a). For instance, the transformation of CIPhe and ClFluor slowed down with increasing humidity, whereas the transformation of ClAnt, ClPyr, ClBaA and ClBaP increased with higher humidity levels, with the highest transformation ratio observed at 45 % humidity. Additionally, we found that the impact of humidity on transformation was not consistent for CIPAH congeners

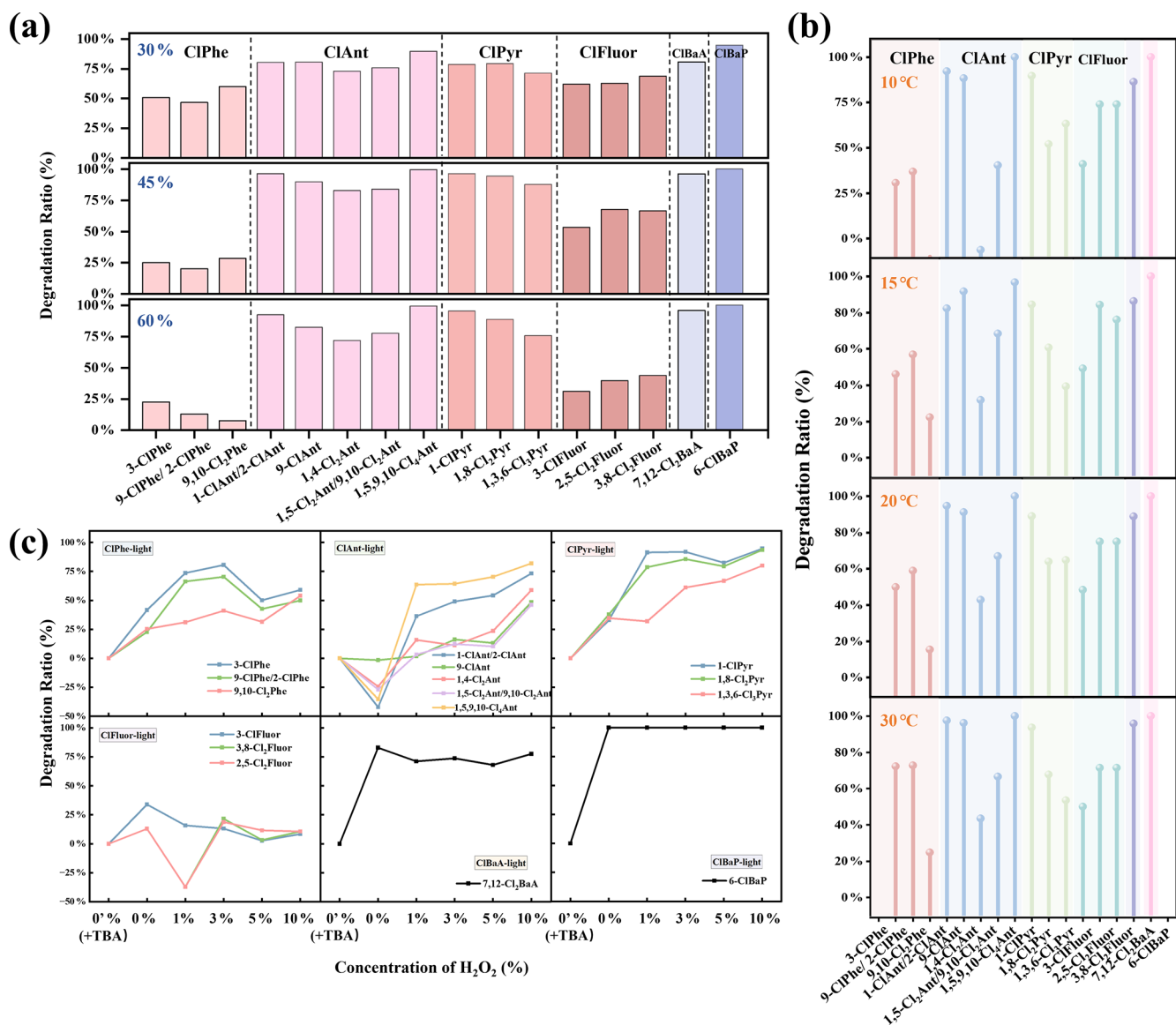


Figure 4. Transformation ratios of CIPAHs under varying (a) humidity levels, (b) temperature conditions and (c) H₂O₂ concentrations, with photoirradiation.

in the same homologue groups. For example, the transformation of 9,10-Cl₂Phe decreased more sharply than the other CIPhe congeners with the increment of humidity. The combined influence of photoirradiation and humidity enhanced the transformation of individual CIPAHs (Fig. S6). For example, under 45% humidity, CIPyr exhibited an average transformation of 50% in darkness, while this rate increased to 75% under photoirradiation. Possible reasons for this could be that the addition of photoirradiation drove the formation of the hydroxyl radical (\bullet OH), which could participate in the breakdown of molecules (Zhang et al., 2023). In contrast, the acceleration of transformation with increasing humidity was relatively universal for BrPAHs, with the most significant

effects observed within the 30%–45% humidity range (Fig. S6c and d).

Transformation ratios of XPAHs increased as temperatures rose, with the most significant transformation observed at 30°C (Fig. 4b), indicating that an elevated temperature promotes the transformation of XPAHs. The transformation ratio of each congener gradually increased with temperature compared with dark conditions (Fig. S7a). Under photoirradiation at the same temperature, the transformation ratios of nearly all XPAH congeners increased by more than 50% compared with dark conditions. This indicated that the breakdown of XPAH molecules was enhanced by the photoirradiation. Under both photoirradiation and dark conditions, the transformation ratios of BrPAHs (Fig. S7c and d) exceeded

those of CIPAHs. This phenomenon can be attributed to the differences in bond strength (the bond energy of C–Br is lower at 291 kJ mol^{-1} , whereas the bond energy of C–Cl is 345 kJ mol^{-1}) (Ohura et al., 2009) and atomic size (the radius of the Cl atom is approximately 99 pm, whereas the radius of the Br atom is around 114 pm) (Shannon, 1976). Adding H_2O_2 to the reaction system simulates the effects of oxidants present in the atmosphere on the impact of XPAH transformation under photochemical conditions. The transformation of CIPAHs accelerated with the increase in the H_2O_2 concentration (Figs. 4c and S8). TBA was introduced to eliminate the $\cdot\text{OH}$ effect in the control group. Under 1 h photoirradiation conditions, the transformation rate ranking of CIPAHs was as follows: ClBaP > ClBaA > ClPyr > ClPhe > ClAnt > ClFluor. The transformation of ClFluor showed no significant change with H_2O_2 content, indicating relative stability. Additionally, compared with monochlorinated compounds, the overall transformation ratios of polychlorinated compounds are relatively slower and less influenced by H_2O_2 (except for 1,5,9,10-Cl₄Ant). This also suggested that the dechlorination process was more pronounced in high-chlorine-number compounds, while the transformation of low-chlorine-number substances was mainly due to ring-opening reactions. The situation was similar for Br-PAHs, with transformation rates faster than those of CIPAHs.

3.5 Heterogeneous transformation pathways of XPAHs under photoirradiation conditions

According to the results above, the processes of dechlorination, direct ring-opening, or ring-opening induced by oxidation are involved in the breakdown of XPAHs. To elucidate the specific transformation pathways of XPAHs, we conducted photolysis experiments on highly chlorinated XPAHs, including 1,4-Cl₂Ant, 9,10-Cl₂Phe, 1,8-Cl₂Pyr, 2,5-Cl₂Fluor, 7,12-Cl₂BaA and 6-ClBaP, individually. Nontarget analysis was then employed to recognize the transformation products of these congeners. Specific mass spectrums can be found in Fig. S9, and the relative compounds are listed in Table S6. The predominant products were quinones, ketones, hydroxyl-bearing compounds and ring-opened products, consistent with previous findings on PAH phototransformation products (Zhao et al., 2017; Jia et al., 2019). Surprisingly, no chlorinated oxides were detected. Further analysis of the products from experiments on both CIPAHs and BrPAHs revealed no significant differences. As a result, we confirmed a hypothesis proposed in previous studies (Ohura et al., 2009): that the transformation of XPAHs underwent dehalogenation to form PAHs before oxidation.

The transformation pathways are presented in Fig. 5. According to the nontarget analysis results of the photolysis products, the primary products for most CIPAHs, with the exception of ClFluor, were the parent PAHs in the initial step. For ClFluor, the initial step involved not only the dechlorination but also ring-opening, resulting in the generation

of 2,7-dichlorofluorene and 9-chlorofluorene. Research findings have suggested that the primary reactions for the destruction of aromatic compounds in the atmosphere were addition or substitution with $\cdot\text{OH}$ (Dang et al., 2014). At the same time, the substitution of H or Cl in the main structures of CIPAHs or PAHs by $\cdot\text{OH}$ could influence the products of the next steps. Therefore, the subsequent steps might include ring-opening, oxidation or hydrolysis.

Specifically, there were three potential pathways for the transformation of 1,4-Cl₂Ant (Figs. 5a and S9a). In the first pathway, 1,4-Cl₂Ant could undergo substitution by $\cdot\text{OH}$ to form A2 (1,4-dihydroxyanthracene, C₁₄H₁₀O₂), which further oxidized to produce A3 (1,4-anthraquinone, C₁₄H₈O₂). For the second and third pathways, 1,4-Cl₂Ant underwent dechlorination to yield A1 (Ant, C₁₄H₁₀). The subsequent steps were then similar to those of Ant, with oxidation leading to the formation of A4 (9,10-anthracenediol, C₁₄H₁₀O₂) and then further oxidation to A5 (9,10-anthraquinone, C₁₄H₈O₂) as the second pathway. In the third pathway, ring-opening occurred to form A6 (2-methylnaphthalene, C₁₁H₁₀), followed by subsequent chain-breaking ring-opening to form A7 (Nap, C₁₀H₈), A8 (1,2,3,4-tetrahydronaphthalene, C₁₀H₁₂) and A9 (2-methoxyphenol, C₇H₈O₂), ultimately yielding A10 (3-nonanol, C₉H₂₀O) and A11 (3-nonanone, C₉H₁₈O). Similar transformation pathways were observed for 9,10-Cl₂Phe (Figs. 5b and S9b), 1,8-Cl₂Pyr (Figs. 5c and S9c) and 7,12-Cl₂BaA (Figs. 5e and S9e), involving dechlorination to generate PAHs, followed by attack by $\cdot\text{OH}$ to produce phenols, further oxidizing to form quinones, acids and esters. Additionally, 9,10-Cl₂Phe exhibited an additional oxidation pathway involving ring-opening oxidation, yielding B9 (9-fluorenone, C₁₃H₈O), followed by a series of chain-breaking ring-opening reactions to sequentially generate B10 (benzophenone, C₁₃H₁₀O), B11 (3'-methylacetophenone, C₉H₁₀O) and B12 (3-nonanone, C₉H₁₈O). The compound 1,8-Cl₂Pyr also had two additional potential transformation pathways. In the first pathway, uniform cleavage occurred both above and below the pyrene molecule, generating C4 (Nap, C₁₀H₈) and C5 (2-methylnaphthalene, C₁₁H₁₀). In the second pathway, diagonal cleavage resulted in the identification of two products: C6 (2-(2,5-dimethylphenyl)-1,4-dimethylbenzene, C₁₄H₁₄) and C7 (4,4'-dimethyldiphenyl, C₁₄H₁₄). C6 underwent attack by $\cdot\text{OH}/\text{O}_2^-$ radicals to ultimately form C8 (benzophenone, C₁₃H₁₀O), followed by further ring-opening cleavage to produce C9 (3'-methylacetophenone, C₉H₁₀O). Similarly, C10 (2-phenylpropionaldehyde, C₉H₁₀O) was formed by oxidation-induced chain-breaking of C8.

For ClFluor (Figs. 5d and S9d), the initial step involved ring-opening, generating D1 (2,7-Cl₂Fle, C₁₃H₈Cl₂) and D2 (9-ClFle, C₁₃H₉Cl). Subsequent dechlorination and ring-opening led to the formation of D3 (4,4'-dimethyldiphenyl, C₁₄H₁₄), D4 (2-(2,5-dimethylphenyl)-1,4-dimethylbenzene, C₁₄H₁₄) and D5 (benzophenone, C₁₃H₁₀O) in the samples.

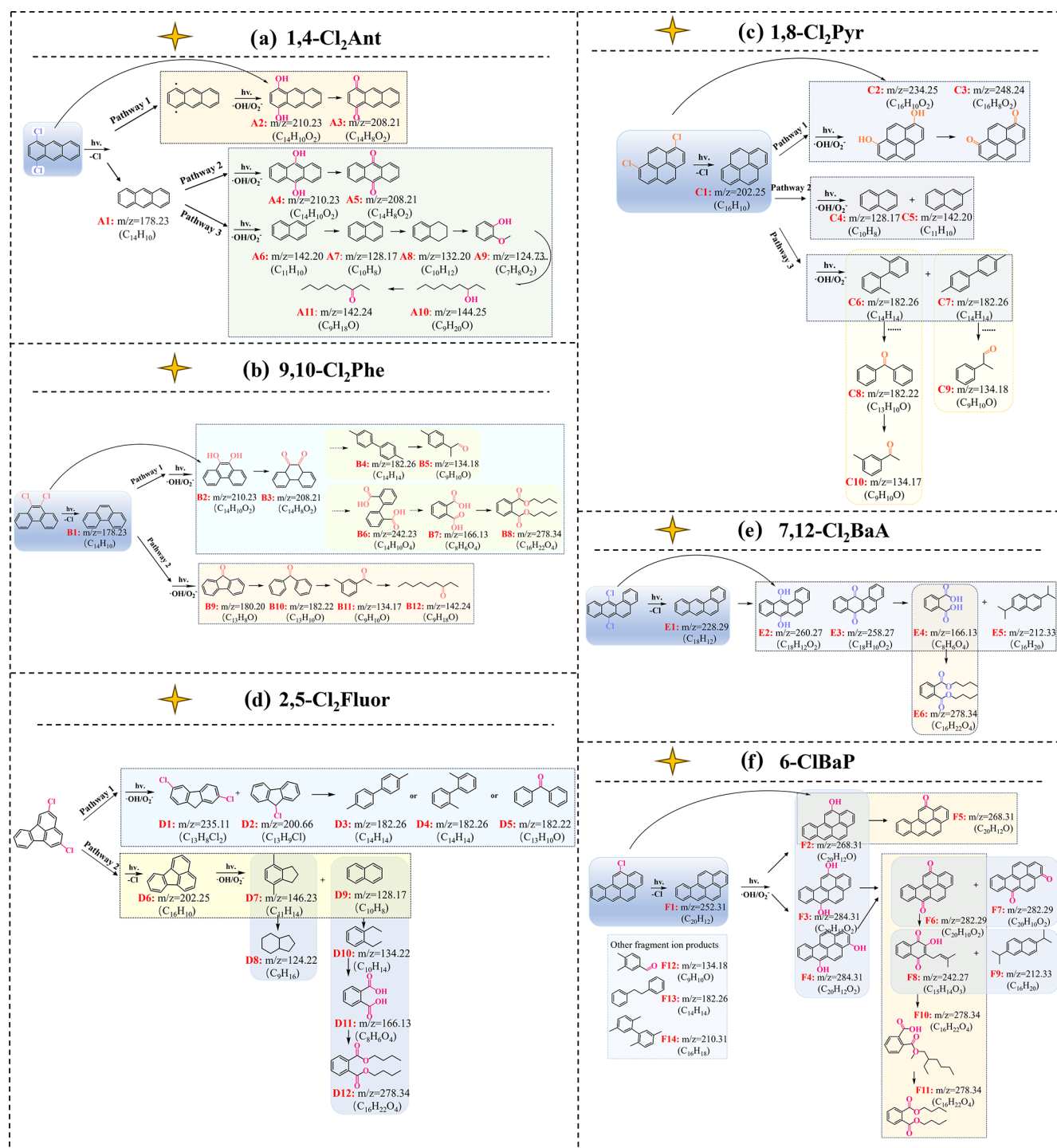


Figure 5. The transformation pathways and relative products of CIPAHs: (a) 1,4-Cl₂Ant; (b) 9,10-Cl₂Phe; (c) 1,8-Cl₂Pyr; (d) 2,5-Cl₂Fluor; (e) 7,12-Cl₂BaA; (f) 6-ClBaP.

In the second pathway, the initial dechlorination process resulted in the formation of D6 (Fluor, C₁₆H₁₀), which yielded D7 (1H-indene, 2,3-dihydro-4,7-dimethyl-, C₁₁H₁₄) and D9 (Nap, C₁₀H₈). D7 underwent bond cleavage to form D8 (1H-indene, octahydro-, C₉H₁₆), while D10 (1,2-diethylbenzene, C₁₀H₁₄) was the ring-opening product of D9. Further oxidation (alcohol to aldehyde) sequentially yielded D11 (1,2-dicarboxybenzene, C₈H₆O₄) and D12 (dibutyl phthalate, C₁₆H₂₂O₄).

C₁₀H₁₄) was the ring-opening product of D9. Further oxidation (alcohol to aldehyde) sequentially yielded D11 (1,2-dicarboxybenzene, C₈H₆O₄) and D12 (dibutyl phthalate, C₁₆H₂₂O₄).

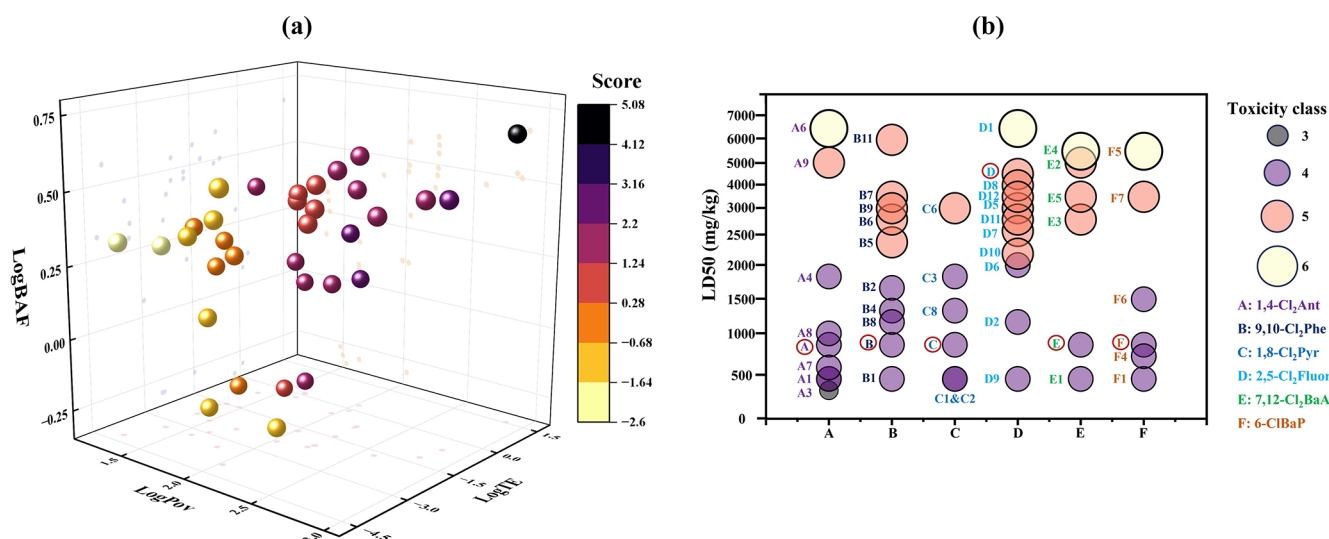


Figure 6. (a) Prediction of environmental behaviors of XPAHs and their transformation products. (b) Respiratory toxicities (LD₅₀) of XPAHs and their transformation products predicted by the ProTox 3.0 model.

The compound 6-ClBaP, as a mono-chlorinated compound (Figs. 5f and S9f), exhibited the highest phototransformation ratio among all ClPAH congeners. After dechlorination, the initial step generated F1 (BaP, C₂₀H₁₂). Among them, positions 3, 6 and 12 of BaP were particularly reactive, and •OH attacks led to the formation of F2, F3 and F4 (6-benzo[a]pyrenol, 6,12-dihydroxybenzo[a]pyrene and 9,12-dihydroxybenzo[a]pyrene, C₂₀H₁₂O), subsequently further generating F5, F6 and F7 (6-benz[a]pyrene, benzo[a]pyrene-6,12-dione and benzo[a]pyrene-3,6-dione, C₂₀H₁₀O₂). Under light exposure, F6 underwent further oxidation and ring-opening to produce F8 (lapachol, C₁₅H₁₄O₃), F9 (2,6-diisopropyl-naphthalene, C₁₆H₂₀) and F11 (dimethyl phthalate, C₁₆H₂₂O₄), as reported by Zhao et al. (2017). The exploration of XPAH transformation is limited by the absence of quantification of the products. Further studies are necessary to elucidate the specific molecular assignments.

3.6 Assessments of persistence, bioaccumulation, long-range transportation, and toxicities of XPAHs and their transformation products

Studies have suggested that transformation products of organic pollutants might exhibit distinct environmental behaviors and heightened ecological toxicity (Zhang et al., 2023). For the assessed P-B-LRTP scores of XPAHs and their transformation products in this study (Fig. 6a and Table S6), it could be observed that, as the transformation pathways progressed, the scores of the transformation products decreased. For instance, the score of 9,10-Cl₂Phe was 5.07, which decreased to 2.13 after dechlorination, and further oxidation products have even lower scores, ranging from 1.65 to −1.27 (9,10-difluorenylquinone to 1,2-benzenedicarboxylic

acid). However, there were also transformation products with relatively high scores, such as B9 (9H-fluorene-9-one; score: 1.57) and B10 (benzophenone; score: 1.81), which warrant special attention in future studies.

To further investigate the toxicities of these transformation products, the lethal doses (LD₅₀ values) and toxicity levels (Fig. 6b and Table S7) were predicted by the respiratory toxicity model in ProTox 3.0 (Banerjee et al., 2024). The findings indicated that the LD₅₀ values of the products generally increased as the transformation pathways progressed, except for 2,5-Cl₂Fluor, indicating a general toxicity decrement alongside XPAH transformation. For instance, the LD₅₀ of 9,10-Cl₂Phe was 886 mg kg^{−1} with a toxicity level of 4. Among its transformation products, only B1 (Phe) had an LD₅₀ (316 mg kg^{−1}, level 4) lower than that of 9,10-Cl₂Phe, while the toxicities of other oxidation and ring-opening products were lower. However, previous studies on the aryl hydrocarbon receptor activities of XPAHs in yeast assays reported the opposite results on toxicities of 9,10-Cl₂Phe and Phe: the relative equivalent potency of 9,10-Cl₂Phe was found to be much higher than Phe. In the case of 2,5-Cl₂Fluor, its inherently high LD₅₀ (4220 mg kg^{−1}, level 5) resulted in most of its products having higher toxicity levels compared with the parent compound. Overall, most transformation products have toxicity levels lower than their precursors. However, given the disparities between model predictions and experimental results, further toxicity experiments are needed to substantiate the changes in toxicity during the transformation process of XPAHs.

4 Conclusion

In summary, this study elucidated the mechanisms, influencing factors, pathways and products involved in the conversion of XPAHs on PM through comprehensive field sampling and laboratory simulations. Experimental findings revealed that the molecular structures of PAHs exerted a significant influence on the conversion process, with dehalogenation and cleavage of the parent ring structure being prominent features of XPAHs conversion. The number and position of substituents further modulated the conversion dynamics. Key environmental parameters, including humidity, temperature and H₂O₂ concentration, were identified as critical factors impacting conversion efficiency. The resulting conversion products and pathways were systematically hypothesized and confirmed, indicating a progressive decrease in the environmental risk associated with the products as conversion advanced. This study provided novel insights into the heterogeneous conversion mechanisms of XPAHs on particulate matter, offering valuable contributions to the understanding of their environmental behavior and impact.

Data availability. All data are available from the corresponding author (Rong Jin – jinrong@ucas.ac.cn) upon request.

Supplement. The Supplement includes detailed information on chemicals, sample testing and analysis data; the screening of chemical properties and toxicity prediction information; the relevant parameters and data from simulation experiments; and chromatograms for product identification. The supplement related to this article is available online at <https://doi.org/10.5194/acp-25-3981-2025-supplement>.

Author contributions. YY, RJ and MZ conceived of the study and wrote the paper, YY, YL, GZ, SZ and XL performed the measurements and collected data. All authors contributed to the data analysis and review of the paper.

Competing interests. The contact author has declared that none of the authors has any competing interests.

Disclaimer. Publisher's note: Copernicus Publications remains neutral with regard to jurisdictional claims made in the text, published maps, institutional affiliations, or any other geographical representation in this paper. While Copernicus Publications makes every effort to include appropriate place names, the final responsibility lies with the authors.

Financial support. This research has been supported by the Natural Science Foundation of Zhejiang Province (grant no. LQ22B070009); the National Natural Science Foundation of

China (grant no. 22106030); the “Pioneer” and “Leading Goose” R&D Program of Zhejiang (grant no. 2023C03157); and the Research Funds of Hangzhou Institute for Advanced Study, UCAS (grant nos. 2023HIAS-Y014, 2022ZZ01017).

Review statement. This paper was edited by Allan Bertram and reviewed by Ahsan Habib and one anonymous referee.

References

- Banerjee, P., Kemmler, E., Dunkel, M., and Preissner, R.: ProTox 3.0: a webserver for the prediction of toxicity of chemicals, *Nucl. Acids Res.*, 52, W513–W520, <https://doi.org/10.1093/nar/gkac303>, 2024.
- Cao, Q., Liu, Y., Lyu, K., Yu, Y., Li, D. H. W., and Yang, L.: Solar Radiation Zoning and Daily Global Radiation Models for Regions with Only Surface Meteorological Measurements in China, *Energ. Convers. Manage.*, 225, 113447, <https://doi.org/10.1016/j.enconman.2020.113447>, 2020.
- Concha, C. and Manzano, C. A.: Priority pesticides in Chile: Predicting their environmental distribution, bioaccumulation, and transport potential, *Integr. Environ. Asses.*, 19, 676–683, <https://doi.org/10.1002/ieam.4680>, 2023.
- Dang, J., Shi, X., Zhang, Q., Hu, J., Chen, J., and Wang, W.: Mechanistic and Kinetic Studies on the OH-Initiated Atmospheric Oxidation of Fluoranthene, *Sci. Total Environ.*, 490, 639–646, <https://doi.org/10.1016/j.scitotenv.2014.04.134>, 2014.
- Deng, Q. X., Feng, J. R., Gao, P. P., and Ni, H. G.: Combined effects of vehicles and waste incineration on urban air halogenated and parent polycyclic aromatic hydrocarbons, *Environ. Int.*, 171, 107720, <https://doi.org/10.1016/j.envint.2022.107720>, 2023.
- Hu, W., Liu, D., Su, S., Ren, L., Ren, H., Wei, L., Yue, S., Xie, Q., Zhang, Z., Wang, Z., Yang, N., Wu, L., Deng, J., Qi, Y., and Fu, P.: Photochemical Degradation of Organic Matter in the Atmosphere, *Adv. Sustain. Syst.*, 5, 2100027, <https://doi.org/10.1002/adsu.202100027>, 2021.
- Jia, H., Zhao, S., Shi, Y., Zhu, K., Gao, P., and Zhu, L.: Mechanisms for Light-Driven Evolution of Environmentally Persistent Free Radicals and Photolytic Degradation of PAHs on Fe(III)-Montmorillonite Surface, *J. Hazard. Mater.*, 362, 92–98, <https://doi.org/10.1016/j.jhazmat.2018.09.019>, 2019.
- Jin, R., Zheng, M., Yang, H., Yang, L., Wu, X., Xu, Y., and Liu, G.: Gas–particle phase partitioning and particle size distribution of chlorinated and brominated polycyclic aromatic hydrocarbons in haze, *Environ. Pollut.*, 231, 1601–1608, <https://doi.org/10.1016/j.envpol.2017.09.066>, 2017a.
- Jin, R., Liu, G., Zheng, M., Jiang, X., Zhao, Y., Yang, L., Wu, X., and Xu, Y.: Secondary Copper Smelters as Sources of Chlorinated and Brominated Polycyclic Aromatic Hydrocarbons, *Environ. Sci. Technol.*, 51, 7945–7953, <https://doi.org/10.1021/acs.est.7b02031>, 2017b.
- Jin, R., Liu, G., Jiang, X., Liang, Y., Fiedler, H., Yang, L., Zhu, Q., Xu, Y., Gao, L., Su, G., Xiao, K., and Zheng, M.: Profiles, Sources and Potential Exposures of Parent, Chlorinated and Brominated Polycyclic Aromatic Hydrocarbons in Haze Associated Atmosphere, *Sci. Total. Environ.*, 593–594, 390–398, <https://doi.org/10.1016/j.scitotenv.2017.03.134>, 2017c.

- Jin, R., Yang, L., Zheng, M., Xu, Y., Li, C., and Liu, G.: Source identification and quantification of chlorinated and brominated polycyclic aromatic hydrocarbons from cement kilns co-processing solid wastes, *Environ. Pollut.*, 242, 1346–1352, <https://doi.org/10.1016/j.envpol.2018.08.025>, 2018.
- Jin, R., Zheng, M., Lammel, G., Bandowe, B. A. M., and Liu, G.: Chlorinated and Brominated Polycyclic Aromatic Hydrocarbons: Sources, Formation Mechanisms, and Occurrence in the Environment, *Prog. Energ. Combust.*, 76, 100803, <https://doi.org/10.1016/j.pecs.2019.100803>, 2020.
- Jin, R., Liu, G., Zhou, X., Zhang, Z., Lin, B., Liu, Y., Qi, Z., and Zheng, M.: Analysis of Polycyclic Aromatic Hydrocarbon Derivatives in Environment, *TrAC-Trend. Anal. Chem.*, 160, 116942, <https://doi.org/10.1016/j.trac.2023.116942>, 2023.
- Kakimoto, K., Nagayoshi, H., Konishi, Y., Kajimura, K., Ohura, T., Hayakawa, K., and Toriba, A.: Atmospheric chlorinated polycyclic aromatic hydrocarbons in East Asia, *Chemosphere*, 111, 40–46, <https://doi.org/10.1016/j.chemosphere.2014.03.072>, 2014.
- Kang, Q., Bao, S., and Chen, B.: Phototransformation of Three Polychlorinated Naphthalenes on Surface of Atmospheric Particulate Matter, *J. Hazard. Mater.*, 409, 124895, <https://doi.org/10.1016/j.jhazmat.2020.124895>, 2021.
- Kitazawa, A., Amagai, T., and Ohura, T.: Temporal Trends and Relationships of Particulate Chlorinated Polycyclic Aromatic Hydrocarbons and Their Parent Compounds in Urban Air, *Environ. Sci. Technol.*, 40, 4592–4598, 2006.
- Lara, S., Villanueva, F., Martín, P., Salgado, S., Moreno, A., and Sánchez-Verdú, P.: Investigation of PAHs, Nitrated PAHs and Oxygenated PAHs in PM₁₀ Urban Aerosols. A Comprehensive Data Analysis, *Chemosphere*, 294, 133745, <https://doi.org/10.1016/j.chemosphere.2022.133745>, 2022.
- Laskin, A., Laskin, J., and Nizkorodov, S. A.: Chemistry of Atmospheric Brown Carbon, *Chem. Rev.*, 115, 4335–4382, <https://doi.org/10.1021/cr5006167>, 2015.
- Li, X., Abdullah, L. C., Sobri, S., Md Said, M. S., Husain, S. A., Aun, T. P., and Hu, J.: Long-Term Air Pollution Characteristics and Multi-scale Meteorological Factor Variability Analysis of Mega-mountain Cities in the Chengdu-Chongqing Economic Circle, *Water Air Soil Poll.*, 234, 328, <https://doi.org/10.1007/s11270-023-06279-8>, 2023.
- Liu, Q., Liggio, J., Li, K., Lee, P., and Li, S. M.: Understanding the Impact of Relative Humidity and Coexisting Soluble Iron on the OH-Initiated Heterogeneous Oxidation of Organophosphate Flame Retardants, *Environ. Sci. Technol.*, 53, 6794–6803, <https://doi.org/10.1021/acs.est.9b01758>, 2019a.
- Liu, Q., Xu, X., Wang, L., Lin, L., and Wang, D.: Simultaneous Determination of Forty-Two Parent and Halogenated Polycyclic Aromatic Hydrocarbons Using Solid-Phase Extraction Combined with Gas Chromatography-Mass Spectrometry in Drinking Water, *Ecotox. Environ. Safe.*, 181, 241–247, <https://doi.org/10.1016/j.ecoenv.2019.06.011>, 2019b.
- Ma, J., Chen, Z., Wu, M., Feng, J., Horii, Y., Ohura, T., and Kanran, K.: Airborne PM_{2.5}/PM₁₀-Associated Chlorinated Polycyclic Aromatic Hydrocarbons and Their Parent Compounds in a Suburban Area in Shanghai, China, *Environ. Sci. Technol.*, 47, 7615–7623, <https://doi.org/10.1021/es400338h>, 2013.
- Malecha, K. and Nizkorodov, S.: Photodegradation of Secondary Organic Aerosol Particles as a Source of Small, Oxygenated Volatile Organic Compounds, *Environ. Sci. Technol.*, 50, 9990–9997, <https://doi.org/10.1021/acs.est.6b02313>, 2016.
- Nilsson, U. L. and Ostman, C. E.: Chlorinated polycyclic aromatic-hydrocarbons – Method of analysis and their occurrence in urban air, *Environ. Sci. Technol.*, 27, 1826–1831, <https://doi.org/10.1021/es00046a010>, 1993.
- Nishimura, C., Horii, Y., Tanaka, S., Asante, K. A., Ballesteros Jr., F., Viet, P. H., Itai, T., Takigami, H., Tanabe, S., and Fujimori, T.: Occurrence, Profiles, and Toxic Equivalents of Chlorinated and Brominated Polycyclic Aromatic Hydrocarbons in E-Waste Open Burning Soils, *Environ. Pollut.*, 225, 252–260, <https://doi.org/10.1016/j.envpol.2016.10.088>, 2017.
- Noro, K., Omagari, R., Ito, K., Wang, Q., Sei, K., Miyake, Y., and Amagai, T.: Sampling, Pretreatment, Instrumental Analysis, and Observed Concentrations of Polycyclic Aromatic Hydrocarbons, Polychlorinated Naphthalenes, and Halogenated Polycyclic Aromatic Hydrocarbons: A Review, *TrAC-Trend. Anal. Chem.*, 169, 117384, <https://doi.org/10.1016/j.trac.2023.117384>, 2023.
- Ohura, T., Amagai, T., and Makino, M.: Behavior and Prediction of Photochemical Degradation of Chlorinated Polycyclic Aromatic Hydrocarbons in Cyclohexane, *Chemosphere*, 70, 2110–2117, <https://doi.org/10.1016/j.chemosphere.2007.08.064>, 2008.
- Ohura, T., Savada, K., Amagai, T., and Shinomiya, M.: Discovery of Novel Halogenated Polycyclic Aromatic Hydrocarbons in Urban Particulate Matters: Occurrence, Photostability, and AhR Activity, *Environ. Sci. Technol.*, 43, 2269–2275, 2009.
- Ohura, T., Horii, Y., Kojima, M., and Kamiya, Y.: Diurnal Variability of Chlorinated Polycyclic Aromatic Hydrocarbons in Urban Air, Japan, *Atmos. Environ.*, 81, 84–91, <https://doi.org/10.1016/j.atmosenv.2013.08.044>, 2013.
- Ohura, T., Sakakibara, H., Watanabe, I., Shim, W. J., Manage, P. M., and Guruge, K. S.: Spatial and vertical distributions of sedimentary halogenated polycyclic aromatic hydrocarbons in moderately polluted areas of Asia, *Environ. Pollut.*, 196, 331–340, <https://doi.org/10.1016/j.envpol.2014.10.028>, 2015.
- Sei, K., Wang, Q., Tokumura, M., Miyake, Y., and Amagai, T.: Accurate and Ultrasensitive Determination of 72 Parent and Halogenated Polycyclic Aromatic Hydrocarbons in a Variety of Environmental Samples via Gas Chromatography-Triple Quadrupole Mass Spectrometry, *Chemosphere*, 271, 129535, <https://doi.org/10.1016/j.chemosphere.2021.129535>, 2021.
- Shannon, R. D.: Revised effective ionic radii and systematic studies of interatomic distances in halides and chalcogenides, *Acta Crystallogr. A*, 32, 751–767, <https://doi.org/10.1107/s0567739476001551>, 1976.
- Shiraishi, H., Pilkington, N. H., Otsuki, A., and Fuwa, K.: Occurrence of chlorinated polynuclear aromatic hydrocarbons in tap water, *Environ. Sci. Technol.*, 19, 585–590, <https://doi.org/10.1021/es00137a001>, 1985.
- Shiraiwa, M., Ammann, M., Koop, T., and Pöschl, U.: Gas uptake and chemical aging of semisolid organic aerosol particles, *P. Natl. Acad. Sci. USA*, 108, 11003–11008, <https://doi.org/10.1073/pnas.1103045108>, 2011.
- Sun, J. L., Zeng, H., and Ni, H. G.: Halogenated polycyclic aromatic hydrocarbons in the environment, *Chemosphere*, 90, 1751–1759, <https://doi.org/10.1016/j.chemosphere.2012.10.094>, 2013.
- Takikawa, T., Wang, Q., Omagari, R., Noro, K., Miyake, Y., and Amagai, T.: Development of an Analytical Method for Indoor Polycyclic Aromatic Hydrocarbons and Their

- Halogenated Derivatives by Using Thermal Separation Probe Coupled to Gas Chromatography-Tandem Mass Spectrometry, *Sci. Total Environ.*, 903, 166931, <https://doi.org/10.1016/j.scitotenv.2023.166931>, 2023.
- Vuong, Q. T., Thang, P. Q., Nguyen, T. N. T., Ohura, T., and Choi, S.-D.: Seasonal variation and gas/particle partitioning of atmospheric halogenated polycyclic aromatic hydrocarbons and the effects of meteorological conditions in Ulsan, South Korea, *Environ. Pollut.*, 263, 114592, <https://doi.org/10.1016/j.envpol.2020.114592>, 2020.
- Wang, T., Liu, Y., Deng, Y., Cheng, H., Yang, Y., Feng, Y., Zhang, L., Fu, H., and Chen, J.: Photochemical Oxidation of Water-Soluble Organic Carbon (WSOC) on Mineral Dust and Enhanced Organic Ammonium Formation, *Environ. Sci. Technol.*, 54, 15631–15642, <https://doi.org/10.1021/acs.est.0c04616>, 2020.
- Wang, Y., Su, P., Ge, X., Ren, H., Ma, S., Shen, G., Chen, Q., Yu, Y., and An, T.: Identification of specific halogenated polycyclic aromatic hydrocarbons in surface soils of petrochemical, flame retardant, and electronic waste dismantling industrial parks, *J. Hazard. Mater.*, 436, 129160, <https://doi.org/10.1016/j.jhazmat.2022.129160>, 2022.
- Xia, Z., Idowu, I., Marvin, C., Thomas, P. J., Johnson, W., Francisco, O., Stetefeld, J., Crimmins, B., Fry, M., and Tomy, G. T.: Identification of halogenated polycyclic aromatic hydrocarbons in biological samples from Alberta Oil-Sands Region, *Chemosphere*, 215, 206–213, <https://doi.org/10.1016/j.chemosphere.2018.10.050>, 2019.
- Xie, J., Tao, L., Wu, Q., Lei, S., and Lin, T.: Environmental Profile, Distributions and Potential Sources of Halogenated Polycyclic Aromatic Hydrocarbons, *J. Hazard. Mater.*, 419, 126164, <https://doi.org/10.1016/j.jhazmat.2021.126164>, 2021.
- Yang, L., Shen, J., Zheng, M., Yang, Q., Li, D., and Liu, G.: Occurrence of chlorinated and brominated polycyclic aromatic hydrocarbons from electric arc furnace for steelmaking, *Environ. Pollut.*, 294, 118663, <https://doi.org/10.1016/j.envpol.2021.118663>, 2022a.
- Yang, Y., Liu, G., Zheng, M., Liu, S., Yang, Q., Liu, X., Wang, M., and Yang, L.: Discovery of significant atmospheric emission of halogenated polycyclic aromatic hydrocarbons from secondary zinc smelting, *Ecotoxicol. Environ. Safe.*, 238, 113594, <https://doi.org/10.1016/j.ecoenv.2022.113594>, 2022b.
- Zhang, L., Yan, W., Kohtani, S., Fukuyoshi, S., Hu, M., Nagao, S., and Tang, N.: Promotive Effects of Marine-Derived Dimethyl Sulfoxide on the Photodegradation of Phenanthrene in the Atmosphere, *Sci. Total Environ.*, 926, 171938, <https://doi.org/10.1016/j.scitotenv.2024.171938>, 2024.
- Zhang, L. H., Li, P. J., Gong, Z. Q., and Oni, A. A.: Photochemical behavior of benzo[a]pyrene on soil surfaces under UV light irradiation, *J. Environ. Sci.*, 18, 1226–1232, [https://doi.org/10.1016/s1001-0742\(06\)60067-3](https://doi.org/10.1016/s1001-0742(06)60067-3), 2006.
- Zhang, Q., Wang, Y., Gao, M., Li, Y., Zhao, L., Yao, Y., Chen, H., Wang, L., and Sun, H.: Organophosphite Antioxidants and Novel Organophosphate Esters in Dust from China: Large-Scale Distribution and Heterogeneous Phototransformation, *Environ. Sci. Technol.*, 57, 4187–4198, <https://doi.org/10.1021/acs.est.2c08239>, 2023.
- Zhao, S., Jia, H., Nulaji, G., Gao, H., Wang, F., and Wang, C.: Photolysis of Polycyclic Aromatic Hydrocarbons (PAHs) on Fe³⁺-Montmorillonite Surface Under Visible Light: Degradation Kinetics, Mechanism, and Toxicity Assessments, *Chemosphere*, 184, 1346–1354, <https://doi.org/10.1016/j.chemosphere.2017.06.106>, 2017.
- Zhu, J., Sheng, M., Shang, J., Kuang, Y., Shi, X., and Qiu, X.: Photocatalytic Role of Atmospheric Soot Particles under Visible-Light Irradiation: Reactive Oxygen Species Generation, Self-Oxidation Process, and Induced Higher Oxidative Potential and Cytotoxicity, *Environ. Sci. Technol.*, 56, 7668–7678, <https://doi.org/10.1021/acs.est.2c00420>, 2022.